2001 TAPPI JOURNAL PEER REVIEWED PAPER

X-RAY PHASE-CONTRAST MICROSCOPY OF PAPER

TIMUR E. GUREYEV[*], ROBERT EVANS[**], ANDREW W. STEVENSON[§], DACHAO GAO[§§] AND STEPHEN W. WILKINS[§§§]

[*]Principal Research Scientist, [§]Principal Research Scientist, [§§]Senior Research Scientist, [§§§]Chief Research Scientist, CSIRO Manufacturing Science and Technology, P.B. 33, Clayton South MDC, VIC 3169, Australia

[**]Senior Principal Research Scientist, Cooperative Research Centre for Hardwood Fibre and Paper Science, CSIRO Forestry and Forest Products, P.B. 10, Clayton South MDC, VIC 3169, Australia

ABSTRACT

We report the first results of a feasibility study of in-line hard X-ray phase-contrast microscopy (IXPCM) of paper samples using laboratory microfocus X-ray source. We demonstrate that the phase-contrast techniques may have considerable advantages over conventional absorption-based radiographs for imaging samples consisting mostly of light chemical elements. We analyze the information content and the nature of image contrast in IXPCM and compare it with ordinary and confocal visible light microscopy and beta-radiography.

Application: This work proposes a new method for rapid non-destructive testing of paper samples.

EXECUTIVE SUMMARY

We investigate the applicability of in-line hard X-ray phase-contrast microscopy (IXPCM) for rapid quantitative imaging of paper samples. IXPCM is a novel technique particularly suitable for non-destructive testing of organic materials. This technique does not generally require any sample preparation (such as e.g. staining or sectioning), and can be used for imaging areas of the order of a few square centimeters in a single exposure with up to submicron spatial resolution. The corresponding exposure time can be of the order of seconds, and will be further reduced with the improvement in microfocus X-ray sources and detector technology. The amount of information contained in a typical IXPCM image is very large, which makes them especially useful for the statistically reliable estimation of fiber network parameters such as e.g. fiber size and orientation distribution in a paper sheet. Among other favorable properties of IXPCM is its ability to image the internal structure of thick optically opaque specimen non-destructively. Three-dimensional imaging is also possible using the tomographic approach. In this paper we describe the theoretical basis of IXPCM, explain the exact physical nature of the image contrast,

and then present several experimental results for different paper samples. All the experiments were performed with a laboratory polychromatic microfocus X-ray source. The images were collected using X-ray Imaging Plates. We demonstrate that appropriate numerical processing of the IXPCM images allows one to obtain maps of spatial density distribution and to evaluate various parameters of the fiber network in paper samples.

INTRODUCTION

Many different X-ray analytical methods, including X-ray densitometry, diffractometry, soft X-ray microscopy, X-ray fluorescence and computer tomography, have been used over the years for studying various properties of wood and paper products (see e.g.(*1-6*)). The very first papers on X-rays by W.C.Röntgen already contained the description of experiments investigating X-ray attenuation in wood, paper and cardboard (*1*). Recent papers (*7, 8*) list a number of novel applications of X-ray techniques to the analysis of wood and wood products. These include the study of fungal growth, streaks and stains, environmental impact of anthropogenic inorganic components in trees, metal content in fibers for pulp bleaching, etc.

The feature of X-rays which differentiates them most from other types of electromagnetic radiation is their ability to penetrate through solid objects. This property has primarily guided existing applications of X-ray imaging methods in medicine, biology and material sciences. Since Röntgen's discovery of X-rays in 1895, almost all X-ray images of non-crystalline samples have been obtained and interpreted on the basis of absorption contrast. Absorption contrast appears when X-rays passing through a sample along different paths are differentially absorbed, and the intensity pattern of the emerging beam records the distribution of absorbing materials within the sample. However, in the case of samples consisting mostly of light chemical elements (such as Carbon, Oxygen, Hydrogen, etc.), one often encounters two contradictory requirements. On one hand, only quite hard X-rays (with wavelength of the order of 1 Å or shorter) can effectively penetrate samples thicker than a few millimeters. On the other hand, such hard X-rays display only a weak dependence of absorption on the variation of mass distribution in the sample. This phenomenon is responsible, for example, for the poor contrast of different soft tissues in conventional medical radiographs.

It has been suggested that phase contrast can be used to improve the quality of hard X-ray images of samples consisting of light elements (*9, 10*). Phase contrast appears when rays change their directions usually owing to refraction effects at interfaces inside the sample. For light elements and hard X-rays, phase contrast can be up to several orders of magnitude stronger than the corresponding absorption contrast (*10*). Furthermore, the amount of phase shift experienced by X-rays on passing through a sample is directly proportional to the average electron density along the ray path. This means that the X-ray phase is related to fundamental physical characteristics of the sample in a straightforward and quantitative manner. It implies, in turn, that in-line hard X-ray phase-contrast microscopy (IXPCM) does not require special sample preparation such as sectioning or staining, and can be used for studying samples in their native state. Full three-dimensional IXPCM in the form of phase-contrast X-ray computer tomography has been recently successfully implemented (*11, 12*).

Phase contrast is more difficult to register than absorption contrast, as it does not immediately lead to intensity variations in the beam emerging from the sample. In conventional (visible light) microscopy, optical elements such as lenses or interferometers are used to render phase contrast

visible. In the hard X-ray region, optical elements of high imaging quality (high efficiency and low aberration) are very difficult to manufacture (*13, 14, 11*). X-ray phase-contrast methods using near-perfect silicon crystals as optical elements (*14-16, 11*) have been proposed and implemented, but they suffer from a number of inherent shortcomings which severely limit their practical application.

More recently, the 'in-line' method of hard X-ray phase-contrast imaging (which closely resembles in principle Gabor's in-line holography) has become the subject of considerable interest (*9, 10*). The generic scheme of in-line imaging method is shown in **Figure 1**. Contrast formation in IXPCM is based on the phenomenon of Fresnel diffraction which transforms phase shifts into intensity variations upon a simple act of free-space propagation. Therefore, in this imaging scheme, it is possible to register phase-contrast images at some distance from the sample without the use of any lenses or interferometers. It was thought that only the very expensive synchrotron sources of X-ray radiation were suitable for this method of X-ray imaging, as they can readily provide incident beams with high spatial and temporal coherence (monochromatic plane waves). However, a group from CSIRO, Australia, has demonstrated (*10*) that the same method can be implemented using conventional, albeit microfocus, laboratory X-ray sources. Moreover, the use of microfocus sources has been shown to have some additional advantages such as inherent magnification of the image (*10*) (Figure 1). IXPCM has a very large depth of focus and can produce high-resolution (currently ~1 micron) images over a very large field of view (currently up to several cm^2) in a single exposure (exposure time currently ~1 minute for paper samples).

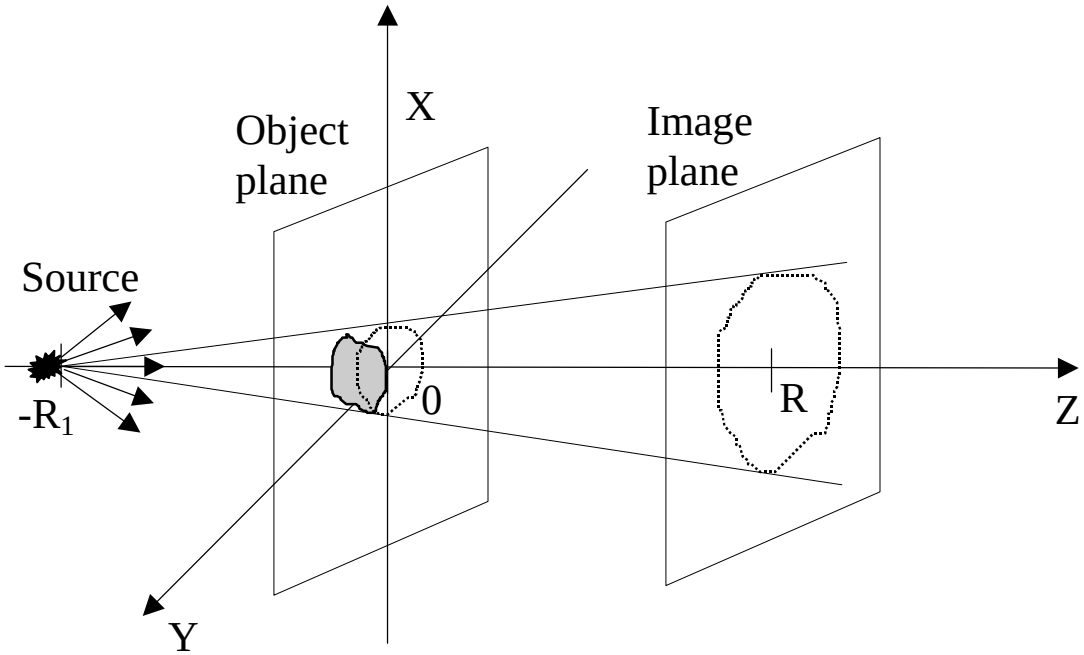

Figure 1. Generic scheme of in-line imaging.

In the present work we study the feasibility of application of IXPCM for the imaging of paper samples using a laboratory polychromatic X-ray source with a source size of about 4 microns. We compare the IXPCM images with ordinary and confocal microscopy images, and also with beta-radiographs obtained using the same paper samples. We show that the type of available

information about the sample is very different in each technique. We also discuss several specific applications of IXPCM images that cannot be easily realized with other analytical methods. These applications include rapid high-resolution densitometry of paper sheets and analysis of various quantitative statistical properties of the fiber network.

THEORETICAL BACKGROUND

Although IXPCM images can be quite informative and reveal fine details of the internal structure of samples, it is important to properly interpret these images in terms of the sample features and the mechanism of Fresnel diffraction. We will show below that the IXPCM images of weakly absorbing objects essentially represent maps of second derivatives (Laplacian) of the X-ray phase distribution in the object plane (*10*). Reconstruction of the phase itself can therefore be achieved by appropriate numerical processing of the in-line images (*17, 10*). In its turn, the X-ray phase distribution in the object plane is directly related to the distribution of electron density in the sample. For the sake of simplicity, we only consider the theory for a monochromatic plane incident wave; the general case of polychromatic and extended sources can be treated similarly with the help of the Fourier frequency-spectrum decomposition (*18*).

Let a plane monochromatic incident X-ray wave with the wavelength $\lambda = 2\pi / k$ propagate along the direction of the optic axis *z*. A weakly scattering object is located in a vicinity of the optic axis immediately before the 'object' plane $z = 0$ (Figure 1). The scalar complex amplitude of the transmitted wave in the object plane can be expressed in terms of its intensity and phase:

$$U_0(x, y) = I^{1/2}(x, y)\exp\{i\varphi(x, y)\}. \qquad (1)$$

The intensity distribution in the object plane, $I(x, y)$, generally reflects the variation of X-ray absorption coefficient in the object. For weakly absorbing objects, the intensity contrast can be negligible, as $I(x, y) = I_0 \exp[-\int \mu(x, y, z')\mathrm{d}z'] \cong I_0$, when the absorption coefficient μ is small, μ <<1. The phase distribution in the object plane, $\varphi(x, y)$, is proportional to the projected electron density, namely

$$\varphi(x, y) = -\lambda r_e \int \rho(x, y, z')\,\mathrm{d}z', \qquad (2)$$

where r_e is the classical electron radius, $\rho(x, y, z)$ is the 3D electron density distribution in the object and integration is performed along the X-ray path through the object. Propagation of the wave Eq.(1) into the empty half-space $z > 0$ can be described by the Fresnel integral, with the intensity distribution in an 'image' plane $z = R$ being equal to

$$I_R(x, y) = \lambda^2 R^{-2} \left| \iint U_0(x', y')\exp\{ik[(x - x')^2 + (y - y')^2]/(2R)\}\,\mathrm{d}x'\mathrm{d}y' \right|^2. \qquad (3)$$

Equation (3) is rather complicated. To facilitate the description of image contrast it may be possible to use the Transport of Intensity Equation (TIE) which is a linear (with respect to the phase) approximation to the Fresnel integral Eq.(3) (*19*). In the case of a weakly absorbing object the TIE takes a very simple form:

$$I_R(x,y) \cong I_0\,[1-(R/k)\,\nabla^2\varphi(x,y)]\,. \qquad (4)$$

Equation (4) implies that the image contrast, $K \equiv (I_R - I_0)/I_0$, directly represents a scaled map of the Laplacian of the projected electron density, i.e.

$$K = -(R/k)\nabla^2\varphi(x,y) = (R\lambda^2 r_e/2\pi)\,\nabla^2[\int \rho(x,y,z')\,\mathrm{d}z']\,. \qquad (5)$$

The general condition for the validity of the approximation Eq.(4) to the full Eq.(3) can be expressed in terms of the wavelength , λ, the object-to-image distance, *R*, and the size of the smallest resolvable feature in the image, *a* : $N_F \equiv a^2/(\lambda R) >> 1$. The definition of the dimensionless quantity N_F essentially coincides with that of the classical Fresnel number. In classical optics, condition $N_F >> 1$ is usually associated with the so-called 'geometrical optics' approximation. In IXPCM the regime described by the condition $N_F >> 1$ is known as the 'outline' mode (*20, 21*). This condition will be fulfilled in the experiments described in the next section of the paper, therefore, the contrast in the images presented there will be interpreted using Eq.(5).

Equation (5) has a mathematical form of a classical Poisson equation and can be used for explicit reconstruction of the phase from the IXPCM images. Boundary conditions necessary for the unambiguous solution of this equation can be defined using simple physical considerations (*17, 19*). The solution, i.e. the recovered phase distribution in the object plane, $\varphi(x,y)$, is directly proportional to the projected electron density in the sample in accordance with Eq.(2). Therefore, this approach allows one to effectively recover the projected electron density distribution. Using the same approach within the framework of conventional computer tomography, one can also reconstruct a quantitative three-dimensional electron density distribution in the sample.

If the thickness of the object in the *z*-direction is constant and the chemical composition is approximately uniform, as e.g. is the case for many paper samples, the distribution of the phase $\varphi(x,y)$ can be naturally interpreted as a map of projected density distribution in the sample. In such a case the contrast in the original IXPCM images can be interpreted as a Laplace-filtered density map. As usual, the Laplace-filtered image emphasizes the edge features (e.g. edges of individual fibers in a paper sheet). In the 'outline' IXPCM images, typically only one dark and one bright Fresnel fringe are visible at edges and interfaces of the sample. At such regions the rapid change in refractive index leads to large values of the Laplacian of the phase, which leads to strong image contrast according to Eq.(5). Regions of the object with slow variation of the refractive index or thickness are imaged with very weak contrast in this regime, as the Laplacian of a slowly varying function is much smaller than the function itself.

EXPERIMENTAL

In this section we present experimental IXPCM images obtained using a laboratory microfocus X-ray source (Feinfocus Röntgen-Systeme GmbH, Garbsen, Germany, Model FXE-225.20 with W target), operating at *V* = 30 kV (voltage) and *I* = 40 μA (current). We also compare these

results with a beta-radiograph and conventional and confocal visible light microscopy images of the same samples. We show the complementary nature of the information obtainable with the use of these experimental techniques, and demonstrate how the IXPCM images can be processed to extract specific quantitative characteristics of the samples.

All images were collected on X-ray Imaging Plates. The source-to-object distance was R_1=100 mm and the object-to-image distance was R = 1900 mm (Figure 1). The exposure time for each image was 60 s. The nominal pixel size in the Imaging Plates was 25 μm and, after taking the geometrical magnification factor of M=20 into account, the effective pixel size in all the paper images was estimated to be 1.25 μm. The spatial resolution, however, was somewhat worse, limited by the nominal X-ray source size of $\sim 3\times 5$ μm^2 (*22*). The difference in the effective source dimensions in the horizontal and vertical directions led to the sometimes noticeable anisotropy in spatial resolution in the images.

Image plates have a number of important advantages compared with X-ray film. Firstly, image plates have higher sensitivity; hence much shorter exposure time is possible. Secondly, image plates have a dynamic range of ~10^5, compared with only ~10^2 for a typical film. Thirdly, the response function of image plates (dependence of grey level on image X-ray dose) is linear, compared with the approximately logarithmic response for film. The linearity of the response function makes it possible to perform truly quantitative analysis of the images. Note also that a typical paper image collected in a single exposure had the physical size of $\sim 25\times 20$ cm^2, which, at M=20, corresponded to an area of $\sim 1.25\times 1.0$ cm^2 on the sample. Such images contained $\sim 10{,}000\times 8{,}000$ 16-bit pixels. The amount of information contained in such images is extremely large, which makes them potentially very useful for statistical analysis of the structure of paper samples. Each image was160 Mb in standard uncompressed TIFF format, and so cannot possibly be presented on a journal page with any reasonable resolution. Therefore, all figures in this paper represent only small subimages with linear dimensions typically of the order of 1,000 pixels.

Figure 2 shows an X-ray subimage of a newsprint. Individual fibers are seen as pairs of approximately parallel lines corresponding to their boundaries, which is typical for differential phase contrast and agrees well with Eq.(5). The lack of contrast between the grey levels in the interior and exterior of fibers indicates the weakness of absorption contrast which is to be expected at the high X-ray energies used in the experiment. The overall contrast and signal-to-noise level are not very high. This problem may be overcome in future by collecting and adding multiple image frames, just as it is done in visible light microscopy with the use of CCDs.

Figure 3 presents an X-ray image of a paper towel with a vertical edge of the towel visible on the left side. A single fiber protruding from the edge of the sample can also be seen with high contrast in the left side of the image. The black-white phase contrast, which can be observed at each fiber boundary, is again in agreement with the theoretical formula Eq.(5). According to Eq.(5) the black-white oscillations of image intensity at edge-type features correspond to the second derivative of the functions describing the edge. Among paper images collected so far using the IXPCM with laboratory microfocus sources, paper towel samples displayed the highest contrast. We believe that this can be explained by the fact that paper towel contains a large proportion of uncollapsed softwood fibers which produce sharp phase contrast at their boundaries.

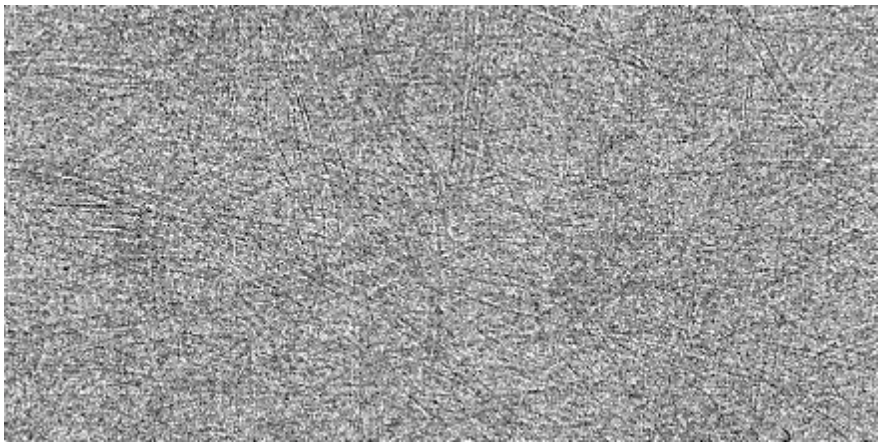

Figure 2. IXPCM image of newsprint.

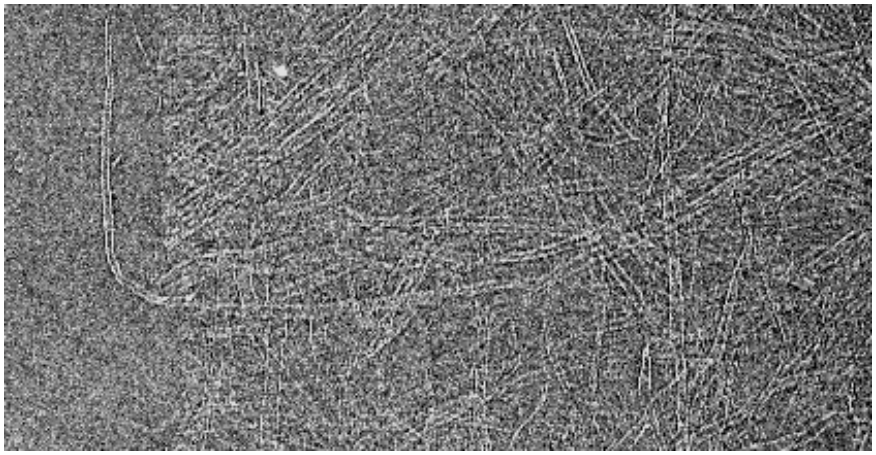

Figure 3. IXPCM image of a paper towel.

Figure 4 presents an IXPCM image of unbleached, kraft, softwood bag paper. Note that the fibers appear more collapsed and ribbon-like than they do in the paper towel. Also, the fibers seem to have a clear preferential orientation along the vertical direction of the image, which probably corresponds to the machine direction of the paper. This orientational anisotropy was expected for this type of paper.

Figures 5, 6 and **7** all depict approximately the same area of a paper towel sample obtained using IXPCM, conventional microscopy in the transmission mode and the confocal laser scanning microscopy in the 'overlaid maximum' projection, respectively. The black broken line drawn over the X-ray image roughly corresponds to the black ink marks visible in the optical images. We also collected confocal images with optical sectioning through the thickness of the sample, however those images did not display much additional information compared with the image in Figure 7. The reason is that in order to obtain IXPCM and confocal images with comparable spatial resolution we had to operate the confocal microscope at a low magnification, thus leading to poor resolution in the *z*-direction. Certainly, confocal microscopy can provide images with much higher magnification and better transverse resolution than that shown in Figure 7. Note however, that the number of pixels in a single image (without X-Y translation of the sample) is approximately a constant, and can be used (together with the dynamic range) as a rough measure

of the information content of the image. In this respect our IXPCM images contained at least 80 times more information than a typical single confocal or conventional microscopy image (with 1024×1024 pixels). It is also worth noting that IXPCM images have all fibers through the thickness of the sample essentially in focus in a single exposure, which is difficult to achieve in conventional or confocal microscopy, especially at higher magnifications.

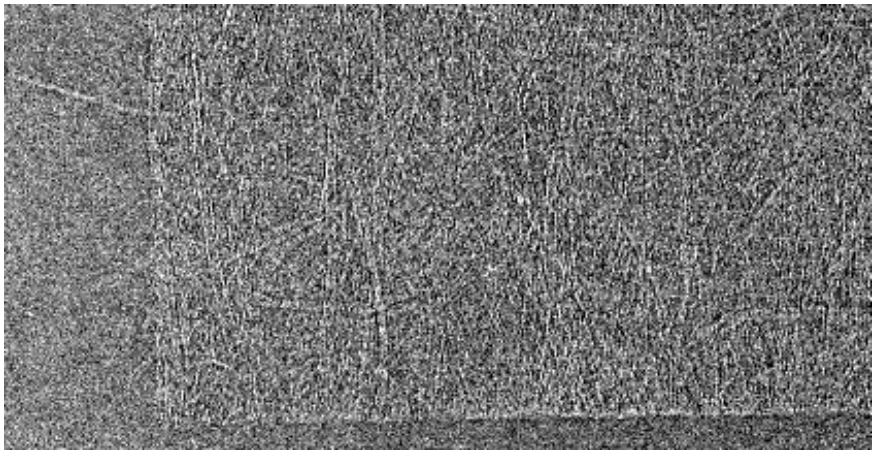

Figure 4. IXPCM image of a paper bag.

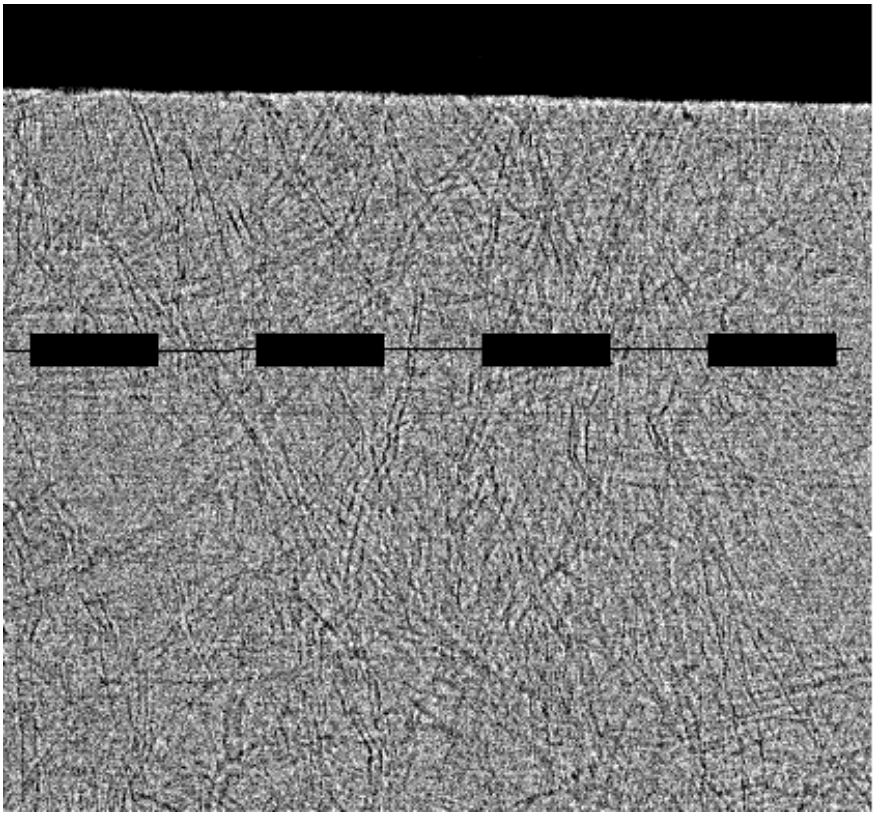

Figure 5. IXPCM image of a paper towel.

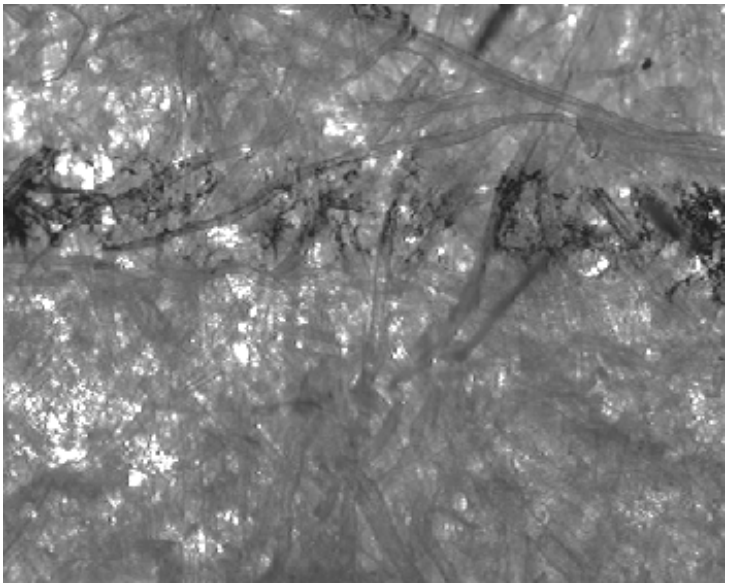

Figure 6. Transmission optical microscopy image of a paper towel.

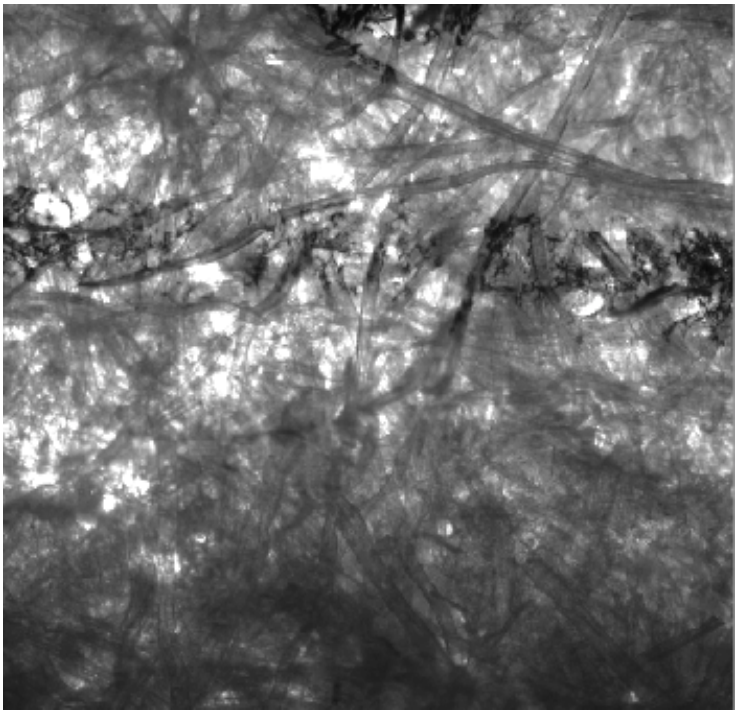

Figure 7. Confocal microscopy image of a paper towel.

Figure 8 is a beta-radiograph collected using the AMBERTEC instrument. This figure represents the variations of density in a 50×50 mm^2 area of paper towel at a spatial resolution of 1 mm. Figure 8 may be compared with **Figure 9** which shows a density map of a 10×10 mm^2 area of the same sample obtained by numerical processing of an IXPCM image (similar to Figure 3) using Eq.(5) as described in the previous section. The spatial resolution of the latter density map is of the order of 10 μm. Sharp boundaries between horizontal strips in Figure 9 are the artifacts of numerical processing. It was found that a direct comparison between the density distributions in Figs.8 and 9 is virtually impossible because of the vast difference in the resolution scales and

the fact that the average values of the density over 1×1 mm^2 areas in Figure 9 display very strong dependence on the exact position of each such averaging area due to the oscillatory nature of the density distribution (to appreciate the problem one may consider the average values of sin(x) over a sliding interval much longer than 2π). Note, however, that the density distribution in Figure 9 closely resembles paper density maps obtained by other methods (*2, 23*). The density map Figure 9 can be obtained much faster than with the AMBERTEC.

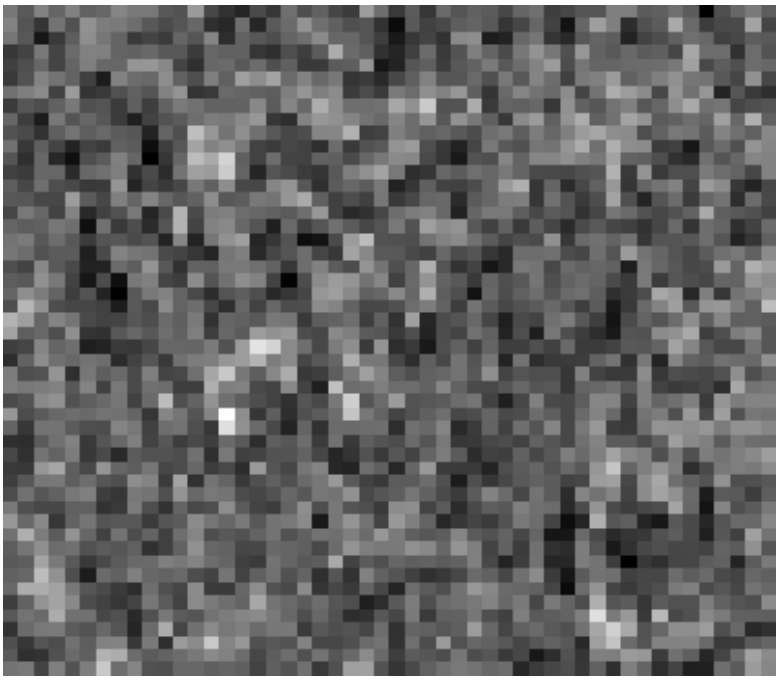

Figure 8. Beta-radiograph of a paper towel.

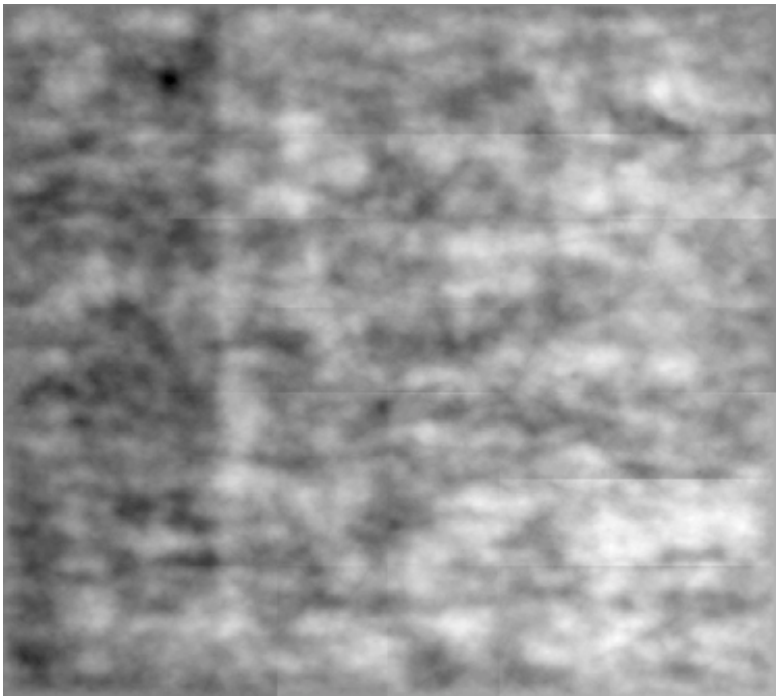

Figure 9. IXPCM phase-reconstructed image of a paper towel.

Figure 10 depicts a part of an IXPCM image of a paper towel sample with fiber boundaries outlined manually (in order to enhance their contrast). **Figure 11** is a grey-scale map of the amplitude of the Fourier transform of Figure 10. Figure 11 demonstrates that some important statistical information about the fiber network can be conveniently extracted from IXPCM images similar to Figure 10. In particular, the relative brightness of each 'ray' extending from the centre of Figure 11 into its periphery corresponds to the relative fraction of fibers in Figure 10 oriented along the direction orthogonal to that 'ray'. The corresponding distribution is shown in **Figure 12**. Note that this distribution is also affected by the X-ray source shape, though its influence can be accounted for.

Another quantity which can be extracted from Figure 11 is the average fiber diameter which corresponds to the radius of the outer boundary of the dark ring around the central area of Figure 11. The corresponding estimation from Figure 11 gave the average fiber diameter equal to 47 μm with a standard deviation of 4 μm. These values would preferentially represent non-collapsed fibers, which have higher contrast in IXPCM images. There are many other quantitative characteristics of paper samples that can be evaluated using IXPCM images (see e.g.(*23*)), though a reliable estimation of those characteristics may be subject to improvement of the signal-to-noise ratio in the IXPCM images obtained using laboratory X-ray sources.

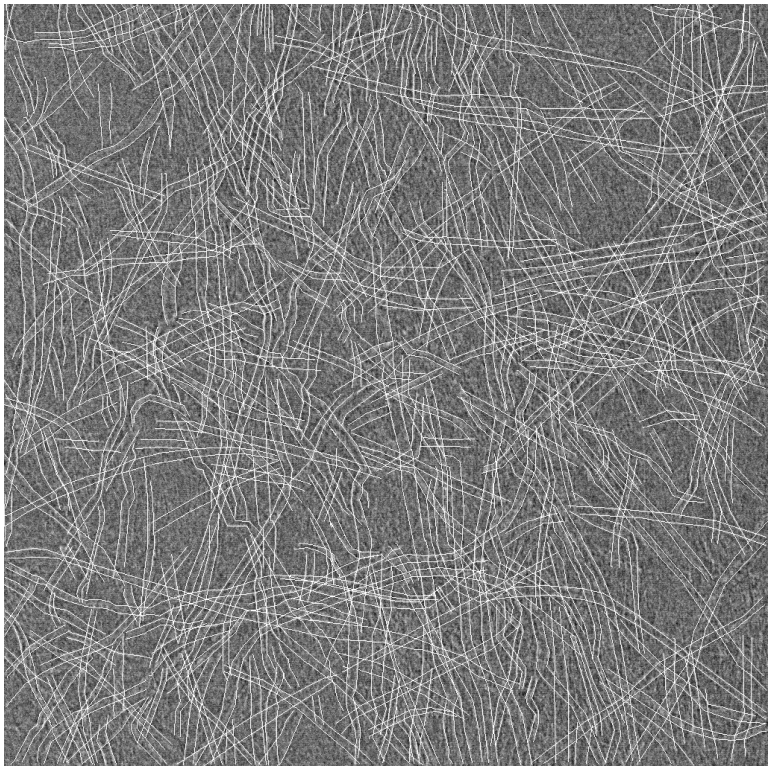

Figure 10. IXPCM image of a paper towel with manually outlined fibers.

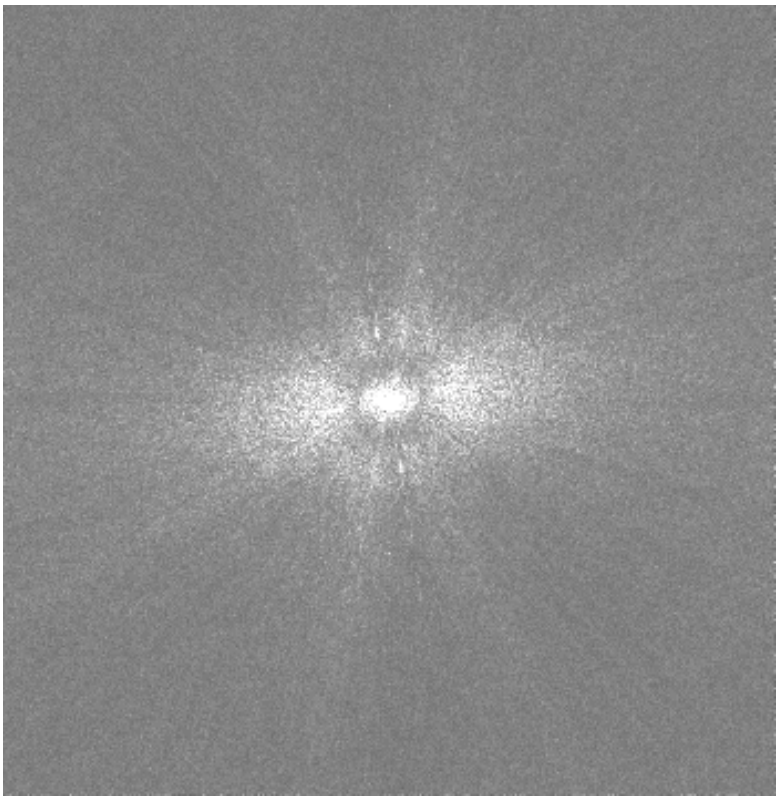

Figure 11. Amplitude of the Fourier transform of Figure 10.

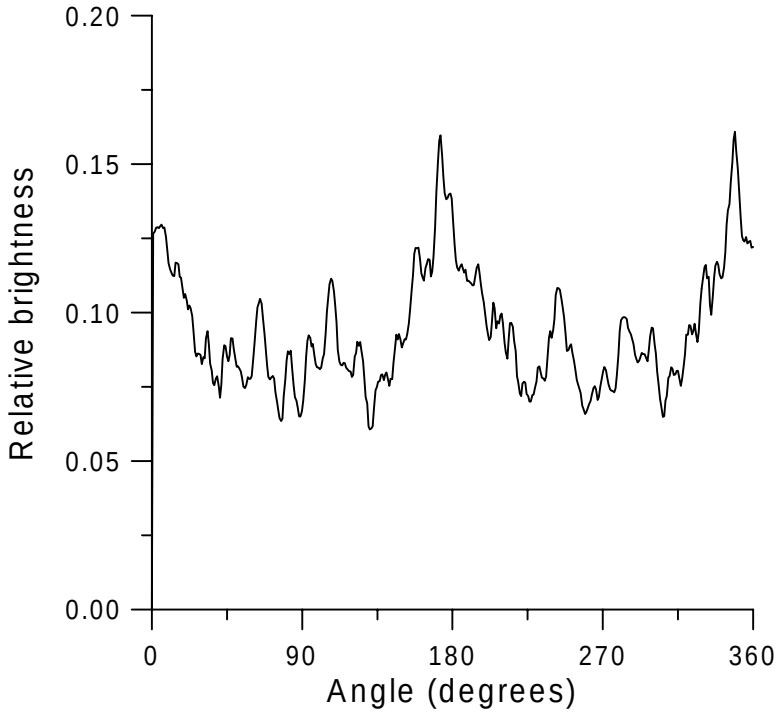

Figure 12. Distribution of brightness of the rays originating from the centre of Figure 11.

CONCLUSIONS

X-ray microscopy can be used for qualitative and quantitative analysis of paper samples. Hard X-ray microscopy has a number of important advantages over other existing imaging techniques such as confocal and conventional optical microscopy, electron microscopy, atomic force microscopy, etc. These advantages include, firstly, the ability to image the internal structure of thick optically opaque objects non-destructively. Secondly, hard X-ray microscopy does not require special preparation of samples (such as sectioning or staining). This leads to the ability to image live samples and monitor *in situ* continuous industrial processes, e.g. paper manufacturing. Thirdly, it is inherently suited to quantitative analysis, allowing measurements of such properties as three-dimensional density distribution, chemical composition, crystallinity, etc. Hard X-ray phase-contrast microscopy is directly sensitive to the electron density distribution throughout the bulk of the sample. This sensitivity of X-ray techniques to basic physical and chemical characteristics, together with established data processing techniques such as computer tomography, indicates considerable potential for the quantitative analysis of wood and paper products. Finally, hard X-ray microscopy offers many different imaging modalities (such as absorption contrast, phase contrast, diffractometry, spectroscopy, secondary electron emission, etc.) which can be used to complement each other. In this report we have presented the first IXPCM images of paper samples using a laboratory microfocus X-ray source. We discussed the theoretical nature and the information content of such images and compared them with the images obtained with visible light microscopy and beta-radiography.

ACKNOWLEDGMENTS

The authors are grateful to Dr. I.Harper (Monash University), Ms. S.Ilic, Dr. K.Orrman-Rossiter (AMCOR R&T) for their help in the course of the present work. A.W.Stevenson, D.Gao and S.W.Wilkins also acknowledge the support of X-Ray Technologies Pty. Ltd.

LITERATURE CITED

1. Röntgen, W. C., *Nature* **53**(1369):274(1896).
2. Newman, S. B. and Fletcher, D., *Tappi J.* **47**(4): 177(1964).
3. Hoag, M. L. and Krahmer, R. L., *Wood and Fiber Sci.* **23**(1): 23(1991).
4. Davis, J. R., Lerdin, A., Wells, P., et al., *J. Inst. Wood Sci.* **12**(4): 259(1991).
5. Evans, R., *Holzforschung* **48**(2): 168(1994).
6. Evans, R., Hughes, M. and Menz, D., *Appita 52nd Annual General Conference Proceedings*, 1998, Brisbane, Australia, p.27.
7. Illman, B. L. and Dowd, B. A., *Synchrotron Radiation News* **10**(2): 18(1997).
8. Rindby, A. and Engström, P., *Highlights 1996/1997, European Synchrotron Radiation Facility*, Grenoble, France, p.79.
9. Snigirev, A., Snigireva, I., Kohn, V., et al., *Rev. Sci. Instrum.* **66**(12): 5486 (1995).
10. Wilkins, S. W., Gureyev, T. E., Gao, D., et al., *Nature (London)* **384**(6607): 335 (1996).
11. Momose, A., Takeda, T. and Itai, Y., *Rev. Sci. Instrum.* **66**(2): 1434(1995).
12. Raven, C., Snigirev, A., Snigireva, I., et al., *Appl. Phys. Lett.* **69**(13): 1826 (1996).
13. Yang, B. X., *Nucl. Instr. Meth. A* **328** : 578(1993).
14. Bonse, U. and Hart, M., *Appl. Phys .Lett.* **7** : 99(1965).
15. Ingal, V. and Belyaevskaya, E. A., *J. Phys. D: Appl. Phys*. **28 :** 2314(1995).

16. Davis, T. J., Gao, D., Gureyev, T. E., et al., *Nature(London)* **373**(6515): 595 (1995).
17. Nugent, K. A., Gureyev, T. E., Cookson, D. F., et al., *Phys. Rev. Lett.* **77**(14): 2961(1996).
18. Gureyev, T. E. and Wilkins, S. W., *Optics Comm.* **147** : 229(1998). [ERRATUM: *Optics Comm.* **154** : 391(1998)].
19. Gureyev, T. E., and Wilkins, S. W., *J. Opt. Soc. Am. A* **15**(3): 579(1998).
20. Snigirev, A. and Raven, C., *Bulletin de la Societe Francaise de Physique* **110**: 10(1997).
21. Gureyev, T. E., Raven, C., Snigirev, A., et al., *J. Physics D.*: *Appl. Phys.* **32**(5) (1999).
22. Pogany, A., Gao, D. and Wilkins, S. W., *Rev. Sci Instrum.* **68**(7): 2774(1997).
23. Nguyen, N. G. and Jordan, B. D., *Paperi ja Puu* **71**(8): 933(1989).

Received: May 13, 1999
Accepted: October 12, 2000

This paper was accepted for abstracting and publication in the February 2001 issue of *TAPPI JOURNAL*.

TAPPI Website: www.tappi.org